

See discussions, stats, and author profiles for this publication at: <https://www.researchgate.net/publication/313886679>

# Improvement of Moving Particle Semi-Implicit Method for Simulation of Progressive Water Waves: Improvement of MPS method for simulation of progressive water waves

Article in International Journal for Numerical Methods in Fluids · February 2017

DOI: 10.1002/fld.4373

---

CITATIONS

5

3 authors, including:



Lizhu Wang

Hohai University

1 PUBLICATION 5 CITATIONS

SEE PROFILE

---

READS

55

# Improvement of moving particle semi-implicit method for simulation of progressive water waves

Lizhu Wang , Qin Jiang\*,† and Changkuan Zhang

*College of Harbor, Coastal and Offshore Engineering, Hohai University, Nanjing 210098, China*

## SUMMARY

Precise simulation of the propagation of surface water waves, especially when involving breaking wave, takes a significant place in computational fluid dynamics. Because of the strong nonlinear properties, the treatment of large surface deformation of free surface flow has always been a challenging work in the development of numerical models. In this paper, the moving particle semi-implicit (MPS) method, an entirely Lagrangian method, is modified to simulate wave motion in a 2-D numerical wave flume preferably. In terms of consecutive pressure distribution, a new and simple free surface detection criterion is proposed to enhance the free surface recognition in the MPS method. In addition, a revised gradient model is deduced to diminish the effect of nonuniform particle distribution and then to reduce the numerical wave attenuation occurring in the original MPS model. The applicability and stability of the improved MPS method are firstly demonstrated by the calculation of hydrostatic problem. It is revealed that these modifications are effective to suppress the pressure oscillation, weaken the local particle clustering, and boost the stability of numerical algorithm. It is then applied to investigate the propagation of progressive waves on a flat bed and the wave breaking on a mild slope. Comparisons with the analytical solutions and experimental results indicate that the improved MPS model can give better results about the profiles and heights of surface waves in contrast with the previous MPS models. Copyright © 2017 John Wiley & Sons, Ltd.

Received 10 January 2016; Revised 18 January 2017; Accepted 20 February 2017

KEY WORDS: improved MPS model; surface detection; corrected gradient model; progressive wave; wave breaking

## 1. INTRODUCTION

The transmission of surface water waves in coastal areas usually involves large surface deformation especially when waves break. Because it is closely related to the design and construction of marine structures, the study on the kinematics of surface waves is of significant importance in coastal engineering. For analyzing nearshore wave characteristics, a great number of numerical models have been developed to simulate the wave motions including wave propagation, transformation, and breaking [1–4]. For free surface flows involving large surface deformation (especially those with fragmentation and coalescence of water, like breaking waves), the accurate calculation of violent surface motion is crucial to a sophisticated numerical model. In traditional grid-based methods, the free surface motion is calculated either by using moveable grids (the arbitrary Lagrangian Eulerian method [5], the boundary-fitted coordinate method [6]), or by introducing auxiliary surface tracking models (the marker and cell method [7], the volume of fluid method

\*Correspondence to: Qin Jiang, College of Harbor, Coastal and Offshore Engineering, Hohai University, Xikang Road 1, Nanjing 210098, China; Tel./Fax.: +86 25 83786539;

†E-mail: qjiang@hhu.edu.cn

[8, 9], the level-set method [10], or the combined models like the coupled level-set and volume of fluid method [11, 12]). However, the former is hard to tackle the problems with violent surface variations because of the grid distortion. And the latter, except for complexities, is hindered in calculation accuracy owing to the numerical diffusions of the advection terms [13], particularly for fluid flows with fragmentation and coalescence.

On the other hand, particle methods, such as the smoothed particle hydrodynamic method [14] and the moving particle semi-implicit (MPS) method [15], have been recently developed and applied in many fields, like mechanical engineering [16], ocean engineering [17, 18], and coastal engineering [19–24]. Different from grid methods, in particle methods, the calculation domain is represented by a set of discrete particles with different physical variables, where the governing equations are discretized by using a certain particles interaction model. The whole control system is then solved by tracing the Lagrangian motion of the discrete particles. Without limitation of the constant topology relationship between particles, the particle methods are inherently suitable for the simulation of fluid flows with violent free surface variations. Moreover, numerical diffusions arisen from the discretization of the advection terms are automatically avoided in particle methods for the adoption of the Lagrangian form of governing equations.

The MPS method was proposed by Koshizuka *et al.* [15, 19] for simulating incompressible fluid flows, which is one of commonly used particle methods. Compared with the conventional grid methods, the MPS method has the advantage on the simplicity of representation of free surfaces, although the stability of initial algorithm is inferior to that of those rigid mesh methods. As the MPS method is gradually applied to practical problems [17, 19, 22], the method itself is amended constantly. For instance, Khayyer and Gotoh [21] modified the gradient model in the original MPS method into an anti-symmetrical form so as to achieve momentum conservation and then investigated the breaking and post-breaking processes of solitary waves on a sloping seabed. Afterwards, Khayyer and Gotoh [25, 26] suggested adopting a pressure gradient models that had higher precision on the basis of Taylor series expansion. Kondo and Koshizuka [27] recommended a multi-term source for pressure Poisson equation (PPE) to alleviate the numerical pressure oscillation. Apart from these, Suzuki *et al.* [28] had ever proposed Hamiltonian moving particle semi-implicit method to improve the problem of nonconservation of mechanical energy in the MPS method. According to the previous researches, the challenges in the MPS method principally reflect on the following aspects: unphysical pressure oscillation [29, 30], particles clustering [31], and nonconservation of momentum and mechanical energy [21, 28]. And the improvements on the MPS method are mostly concentrated on the gradient model, the source term of PPE [29], the Laplacian operator [32], free surface detection, and so on.

The study on surface wave motions is not an unfamiliar topic in the application of MPS method, but the numerical wave damping problem is a barrier for its further development. Early in 1998, Koshizuka *et al.* [19] had simulated breaking waves by the original MPS method in which the issue of numerical wave damping is avoided by choosing a large wavelength compared with the tank length. Iribé and Nakaza [33] successfully decreased the numerical wave dissipation in their progressive wave calculation by introducing a higher precision gradient model. But there was a problem of un-uniform waveforms in the simulated results. Gotoh and Khayyer [34, 35] suggested the Taylor series consistent pressure gradient model to improve the energy conservation in the simulation of wave propagations. In this paper, some modifications based on the original MPS method are put forward to improve the numerical representation of water wave propagations. A vertical 2-D numerical wave flume is constituted with the modified MPS method. A new and simple free surface detection criterion in terms of fluid pressure is proposed to reduce the pressure fluctuations caused by the misrecognition of the free surface particles. And a new pressure gradient model with higher precision is derived from Taylor series expansion analysis. Like the original gradient operator by Koshizuka *et al.* [19], the minimum value of pressure within the active area of a concerning particle is taken into account in the revised pressure gradient model so as to abate the clustering of particles and smooth pressure. The enhancement of improved MPS method is firstly verified by the calculation of hydrostatic problem. The result shows that the modifications are effective to suppress the pressure oscillation and to weaken the local particle clustering. It is then applied to simulate the propagation of regular wave on a flat bottom and the motion of a standing wave and a solitary wave

breaking on a mild slope. The calculated results show that the proposed modifications contribute to the reduction of numerical wave attenuation and the enhancement of total wave energy conversation very well.

## 2. NUMERICAL METHODS

### 2.1. Original moving particle semi-implicit method

In the MPS method [15], the governing equations for incompressible viscous fluid are the equation of continuity and Navier–Stokes equation that are represented as

$$\frac{1}{\rho} \frac{D\rho}{Dt} + \nabla \cdot \mathbf{u} = 0 \quad (1)$$

$$\frac{D\mathbf{u}}{Dt} = -\frac{1}{\rho} \nabla p + \nu \nabla^2 \mathbf{u} + \mathbf{g} \quad (2)$$

where  $\mathbf{u}$  is the velocity vector,  $t$  is the time,  $\rho$  is the density of fluid,  $p$  is the pressure,  $\nu$  is the kinematic viscosity coefficient, and  $\mathbf{g}$  is the gravitational acceleration. The changes of the density of fluid with time  $D\rho/Dt$  is set to zero for incompressible fluid. In the MPS method, the fluid density is replaced by the particle number density, and they are equivalent according to the physical meaning. The particle number density is defined as

$$\langle n \rangle_i = \sum_{j \neq i} w(|\mathbf{r}_j - \mathbf{r}_i|) \quad (3)$$

where  $\mathbf{r}_i$  and  $\mathbf{r}_j$  represent the positions of the target particle and its neighboring particles in the Cartesian coordinate system, respectively. The  $w(r)$  is the kernel function, which is a weight function indicating the degree of interaction between particles. In the MPS method, the physical properties of a target particle are integrated from that of its influential neighboring particles. So the kernel plays a crucial role in the MPS method. The most common kernel function in the MPS method is the one proposed by Koshizuka and Oka [15]:

$$w(r) = \begin{cases} \frac{r_e}{r} - 1 & 0 \leq r < r_e \\ 0 & r_e \leq r \end{cases} \quad (4)$$

where  $r_e$  is the radius of the influential area of surrounding particles to a target particle and  $r$  is the distance between a target particle and its surrounding particles, which is equal to  $|\mathbf{r}_j - \mathbf{r}_i|$ . In this paper, the radius of the particle interaction domain is set to be  $2.1l_0$  for calculating the particle number density and the gradient approximation and set to be  $3.1l_0$  for the Laplacian approximation. Here,  $l_0$  is the initial spatial distance of particle arrangement.

In the MPS method, the discrete differential operators are directly constructed by the interaction relationships between particles. The models for the gradient, Laplacian, and divergence operators are respectively written as

$$\nabla \phi|_i = \frac{D_s}{n_0} \sum_{j \neq i} \frac{\phi_j - \phi_i}{|\mathbf{r}_j - \mathbf{r}_i|^2} (\mathbf{r}_j - \mathbf{r}_i) w(|\mathbf{r}_j - \mathbf{r}_i|) \quad (5)$$

$$\nabla^2 \phi|_i = \frac{2D_s}{n_0 \lambda} \sum_{j \neq i} (\phi_j - \phi_i) w(|\mathbf{r}_j - \mathbf{r}_i|) \quad (6)$$

$$\nabla \cdot \vec{\phi}|_i = \frac{D_s}{n_0} \sum_{j \neq i} \frac{(\vec{\phi} - \vec{\phi}) \cdot (\mathbf{r}_j - \mathbf{r}_i)}{|\mathbf{r}_j - \mathbf{r}_i|^2} w(|\mathbf{r}_j - \mathbf{r}_i|) \quad (7)$$

where  $\phi$  is an arbitrary scalar,  $\vec{\phi}$  is an arbitrary vector,  $D_s$  is the number of dimensions,  $n_0$  is the particle number density constant, and  $\lambda$  is a parameter that is defined as

$$\lambda = \frac{\sum_{j \neq i} |\mathbf{r}_j - \mathbf{r}_i|^2 w(|\mathbf{r}_j - \mathbf{r}_i|)}{\sum_{j \neq i} w(|\mathbf{r}_j - \mathbf{r}_i|)} \quad (8)$$

For solving the discretized calculation system of fluid flows with the MPS method, a fractional step algorithm is adopted, like simplified marker and cell method. First, all the terms in the momentum equation except pressure are calculated explicitly. According to the invariance of particle number density for the incompressible fluid, the PPE is derived, from which the pressure field is solved implicitly. The PPE in the original MPS method is expressed as

$$\nabla^2 p = \frac{\rho_0}{\Delta t^2} \frac{n_0 - n^*}{n_0} \quad (9)$$

where  $n^*$  is an intermediate result of particle number density obtained in the explicit calculation step for the moment equation without pressure term.

Given that the free velocity divergence condition should be satisfied for the incompressible fluid flows, Lee *et al.* [30] suggested adding this restrictive condition to the source term of the given PPE. The PPE can then be expressed as

$$\langle \nabla^2 P \rangle_i^{k+1} = (1 - \gamma) * \rho_0 \frac{\langle \nabla \cdot u \rangle_i^*}{\Delta t} - \gamma * \frac{\rho_0}{(\Delta t)^2} \frac{n_i^* - n_0}{n_0} \quad (10)$$

where  $\gamma$  is a model parameter (0.01 is usually adopted). The main part of the source term is the divergence of temporary velocity, and  $\gamma$  is utilized to stable and smooth the pressure field. After solving the PPE, the final velocity field at a certain time step can be updated with the calculated pressure field.

## 2.2. Improved moving particle semi-implicit method

In this paper, two aspects of modification have been carried out to improve the original MPS method. One is the new and simple free surface detection method, and the other is a more sophisticated and stable pressure gradient model that is obtained by Taylor series expansion analysis.

**2.2.1. Free surface detection.** Simple and efficient treatment of free surface is one of the main shining points in the MPS method. As shown in Figure 1, the influential area of a surface particle is a lack of particles outside of the fluid region that results in its particle number density  $n_i$  is less than the initial density constant  $n_0$ . Because of the difference in particle number density, the original identification criterion for surface particles is defined as

$$n_i < \beta n_0 \quad (11)$$

where  $\beta$  is a coefficient, it usually ranges from 0.8 to 0.97, and  $\beta = 0.95$  is adopted in this paper. The particles that are complying with Eq. (11) are marked as surface particles.

Nevertheless, this oversimplified surface detection method often causes the misrecognition of surface particles. That is to say, when the particles disrupt from the initials regular arrangement, the inner particles have the possibility to be recognized as surface particles. To improve surface

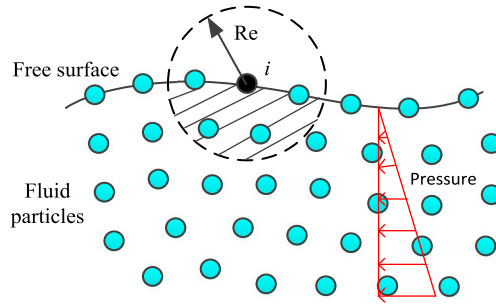


Figure 1. Free surface particles recognition by pressure. [Colour figure can be viewed at [wileyonlinelibrary.com](http://wileyonlinelibrary.com)]

detection precision, Khayyer *et al.* [36] ever put forward an auxiliary criterion for the assessment of surface particles in terms of the principle that neighboring particles distribute in approximately symmetric form around a target particle. Zhang *et al.* [37] ever gave a vector function as an additional condition to increase the accuracy of surface detection. Tanaka and Masunaga [29] suggested a surface particle recognition criterion according to the variation of neighboring particle number  $N_i$  that is expressed as Eq. (12).

$$N_i < \beta N_0 \quad (12)$$

Although this scheme ((12)) is feasible, the calculation of neighboring particle number occupies extra computing cost, and the surface particles near the solid boundary are likely to be misrecognized as inner particles.

In this paper, a new surface particle detection method is proposed, considering that the fluid pressure surrounding a certain particle should be continuous within a very short period of time for a continuous fluid. In other words, after a time increment, the pressure value of a particle is barely possible to change sharply from its previous value, especially under the Courant–Friedrichs–Lewy stability condition. According to the dynamic surface boundary condition, the pressure of surface particles would be equal to the atmospheric pressure ( $P_a = 0$ ). Therefore, only the particle which pressure is less than a certain reference value can be identified as a surface particle. For this reason, an auxiliary criterion for a surface particle by using particle pressure can be established, which is given as

$$P_i^k < P_{ref} \quad (13)$$

$$P_{ref} = \alpha \rho g l_0 \quad (14)$$

Here,  $P_i^k$  is the pressure of particle  $i$  at time step  $k$ . The pressure field calculated in the previous time step is used for pressure evaluation, which needs no additional computing cost. The  $P_{ref}$  depends on the spatial resolution, and  $\alpha$  is a relaxation coefficient, synthesizing the effects of flow pattern. Through hydrostatic tests, the variation of  $\alpha$  barely influences the simulation results if the value of  $\alpha$  is around 1.0. In this paper,  $\alpha$  is chosen as 0.75. And its validity in violent free surface fluid flows also will be manifested by the simulation of dam breaking. The most prominent advantage of this auxiliary assessment criterion is its effectiveness in surface particle identification and its simplicity in implementation. Here, it is necessary to state that the new surface particle detection method with pressure is mainly effective for most of the gravitational flows.

**2.2.2. Pressure gradient model.** As shown in Figure 2, the gradient operator of the original MPS method is derived straightforwardly from a local weighted average of the gradient vectors between the particle  $i$  and its neighboring particle  $j$ . And the gradient vectors between particle  $i$  and its neighboring particles  $j$  are evaluated as  $(\phi_j - \phi_i)(\mathbf{r}_j - \mathbf{r}_i)/|\mathbf{r}_j - \mathbf{r}_i|^2$ . To lessen particles clustering, Koshizuka

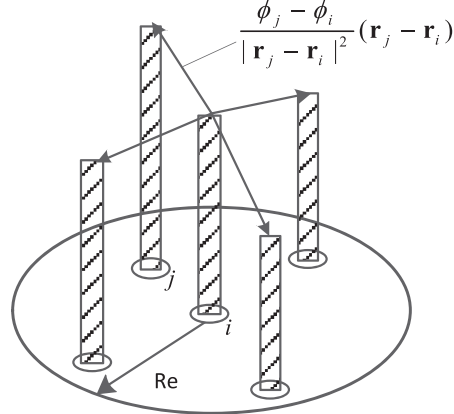


Figure 2. The basic concept of gradient model.

*et al.* replaced  $p_i$  with the minimum value of  $p$  among the neighboring particles in the pressure gradient operator, which can be expressed as

$$\nabla p|_i = \frac{D_s}{n_0} \sum_{j \neq i} \frac{(p_j - \hat{p}_i)}{|r_j - r_i|^2} (r_j - r_i) w(|r_j - r_i|) \quad (15)$$

$$\hat{p}_i = \min_{j \in J} (p_i, p_j) \quad , \quad J = \{j : w(|r_j - r_i|) \neq 0\} \quad (16)$$

Equation (15) is in a very simple form, but it is inferior in the conservation of energy and momentum of fluid flows, which would result in the poor accuracy of the numerical computation. The existing results indicate that this pressure gradient model may cause numerical wave damping. Khayyer and Gotoh [21] constituted an anti-symmetric pressure gradient formulation to keep the conversation of linear momentum. Unfortunately, the perturbation from the boundary may be magnified by the formulation. Toyoda *et al.* [38] suggested an analogous model by adding two  $\phi_i$  to the original gradient equation for representing the action and reaction behavior. However, anti-symmetric models are mainly suitable for simulation of symmetric flows and could not overcome the problem of significant energy damping. To minimize numerical wave damping, many researchers advocated using the Taylor series expansion to deduce a pressure gradient model with a higher precision. For example, Khayyer *et al.* [25, 26] gave their corrected pressure gradient model derived from Taylor series expansion. To increase the stability of the Taylor series pressure gradient model, Tsuruta *et al.* [39] proposed a particle regularization scheme on the basis of Khayyer's gradient model. In terms of these previous contributions, a new pressure gradient model is proposed in this paper, which is also on the basis of Taylor series expansion analysis method. As shown in Eq. (17), the pressure  $p_j$  of the neighboring particle  $j$  can be expressed as the Taylor series about the pressure  $p_i$  of a target particle  $i$ .

$$p_j = p_i + \nabla p|_{ij} \cdot (r_j - r_i) + o(r_{ij}^2) \quad (17)$$

$$\nabla p|_{ij} \cdot (r_j - r_i) = p_j - p_i \quad (18)$$

Neglecting higher-order terms, Eq. (17) can be simplified as Eq. (18) with first-order accuracy. Because the particles  $i$  and  $j$  are unlikely to overlap completely, so  $|r_j - r_i|$  would not be zero, then on both sides of Eq.(17), it can be divided by  $|r_j - r_i|$ . To consider the impact of particles space

distribution, Eq. (19) is multiply by  $(\mathbf{r}_j - \mathbf{r}_i)/|\mathbf{r}_j - \mathbf{r}_i|$  that is the unit vector of the relative displacement between the particles  $i$  and  $j$ .

$$\nabla p|_{ij} \cdot \frac{(\mathbf{r}_j - \mathbf{r}_i)}{|\mathbf{r}_j - \mathbf{r}_i|} = \frac{p_j - p_i}{|\mathbf{r}_j - \mathbf{r}_i|} \quad (19)$$

$$\left( \nabla p|_{ij} \cdot \frac{(\mathbf{r}_j - \mathbf{r}_i)}{|\mathbf{r}_j - \mathbf{r}_i|} \right) \frac{(\mathbf{r}_j - \mathbf{r}_i)}{|\mathbf{r}_j - \mathbf{r}_i|} = \frac{p_j - p_i}{|\mathbf{r}_j - \mathbf{r}_i|} \frac{(\mathbf{r}_j - \mathbf{r}_i)}{|\mathbf{r}_j - \mathbf{r}_i|} \quad (20)$$

Converting the vector of left hand side of Eq. (20) to the form of index notation, Eq. (20) is then rewritten as Eq. (21). The left hand side of Eq. (21) can be regarded as a two-dimensional matrix multiplied by a vector. For simplicity, by using a tensor product for the two-dimension matrix, Eq. (20) can be expressed as Eq. (22).

$$\left( \frac{\frac{\partial p_{ij}}{\partial x} \cdot x_{ij} + \frac{\partial p_{ij}}{\partial y} \cdot y_{ij}}{|\mathbf{r}_j - \mathbf{r}_i|} \right) \frac{[\begin{matrix} x_{ij} & y_{ij} \end{matrix}]}{|\mathbf{r}_j - \mathbf{r}_i|} = \frac{p_j - p_i}{|\mathbf{r}_j - \mathbf{r}_i|} \frac{(\mathbf{r}_j - \mathbf{r}_i)}{|\mathbf{r}_j - \mathbf{r}_i|} \quad (21)$$

$$\left[ \frac{(\mathbf{r}_j - \mathbf{r}_i)}{|\mathbf{r}_j - \mathbf{r}_i|} \otimes \frac{(\mathbf{r}_j - \mathbf{r}_i)^T}{|\mathbf{r}_j - \mathbf{r}_i|} \right] \nabla p|_{ij} = \frac{p_j - p_i}{|\mathbf{r}_j - \mathbf{r}_i|} \frac{(\mathbf{r}_j - \mathbf{r}_i)}{|\mathbf{r}_j - \mathbf{r}_i|} \quad (22)$$

With the principle of weighted average, the pressure gradient model can be written as

$$\left[ \frac{1}{n_0} \sum_{i \neq j} w(|\mathbf{r}_j - \mathbf{r}_i|) \frac{(\mathbf{r}_j - \mathbf{r}_i)}{|\mathbf{r}_j - \mathbf{r}_i|} \otimes \frac{(\mathbf{r}_j - \mathbf{r}_i)^T}{|\mathbf{r}_j - \mathbf{r}_i|} \right] \nabla p|_i = \frac{1}{n_0} \sum_{i \neq j} w(|\mathbf{r}_j - \mathbf{r}_i|) \frac{p_j - p_i}{|\mathbf{r}_j - \mathbf{r}_i|} \frac{(\mathbf{r}_j - \mathbf{r}_i)}{|\mathbf{r}_j - \mathbf{r}_i|} \quad (23)$$

$$\nabla p|_i = \left[ \frac{1}{n_0} \sum_{i \neq j} w(|\mathbf{r}_j - \mathbf{r}_i|) \frac{(\mathbf{r}_j - \mathbf{r}_i)}{|\mathbf{r}_j - \mathbf{r}_i|} \otimes \frac{(\mathbf{r}_j - \mathbf{r}_i)^T}{|\mathbf{r}_j - \mathbf{r}_i|} \right]^{-1} \left[ \frac{1}{n_0} \sum_{i \neq j} w(|\mathbf{r}_j - \mathbf{r}_i|) \frac{p_j - p_i}{|\mathbf{r}_j - \mathbf{r}_i|} \frac{(\mathbf{r}_j - \mathbf{r}_i)}{|\mathbf{r}_j - \mathbf{r}_i|} \right] \quad (24)$$

Learning from Koshizuka (as given in Eq. (15)), the minimum pressure in the local pressure field of the target particle is considered to eliminate local particle clustering and then increase the model stability. Equation (24) can be equivalently transformed as Eq. (25).

$$\begin{aligned} \nabla p|_i &= \left[ \frac{1}{n_0} \sum_{i \neq j} w(|\mathbf{r}_j - \mathbf{r}_i|) \frac{(\mathbf{r}_j - \mathbf{r}_i)}{|\mathbf{r}_j - \mathbf{r}_i|} \otimes \frac{(\mathbf{r}_j - \mathbf{r}_i)^T}{|\mathbf{r}_j - \mathbf{r}_i|} \right]^{-1} \left[ \frac{1}{n_0} \sum_{i \neq j} w(|\mathbf{r}_j - \mathbf{r}_i|) \frac{p_j - \hat{p}_i}{|\mathbf{r}_j - \mathbf{r}_i|} \frac{(\mathbf{r}_j - \mathbf{r}_i)}{|\mathbf{r}_j - \mathbf{r}_i|} \right] \\ &\quad + \left[ \frac{1}{n_0} \sum_{i \neq j} w(|\mathbf{r}_j - \mathbf{r}_i|) \frac{(\mathbf{r}_j - \mathbf{r}_i)}{|\mathbf{r}_j - \mathbf{r}_i|} \otimes \frac{(\mathbf{r}_j - \mathbf{r}_i)^T}{|\mathbf{r}_j - \mathbf{r}_i|} \right]^{-1} \left[ \frac{1}{n_0} \sum_{i \neq j} w(|\mathbf{r}_j - \mathbf{r}_i|) \frac{(\mathbf{r}_j - \mathbf{r}_i)}{|\mathbf{r}_j - \mathbf{r}_i|^2} \right] (\hat{p}_i - p_i) \end{aligned} \quad (25)$$

Assuming the distribution of particles is approximately symmetrical, the second term on the right hand of Eq. (25) approaches to zero. Hence, neglecting this term, Eq. (25) can be simplified as Eq. (26).

$$\nabla p|_i = \left[ \frac{1}{n_0} \sum_{i \neq j} w(|\mathbf{r}_j - \mathbf{r}_i|) \frac{(\mathbf{r}_j - \mathbf{r}_i)}{|\mathbf{r}_j - \mathbf{r}_i|} \otimes \frac{(\mathbf{r}_j - \mathbf{r}_i)^T}{|\mathbf{r}_j - \mathbf{r}_i|} \right]^{-1} \left[ \frac{1}{n_0} \sum_{i \neq j} w(|\mathbf{r}_j - \mathbf{r}_i|) \frac{p_j - \hat{p}_i}{|\mathbf{r}_j - \mathbf{r}_i|} \frac{(\mathbf{r}_j - \mathbf{r}_i)}{|\mathbf{r}_j - \mathbf{r}_i|} \right] \quad (26)$$

The right hand side of Eq. (26) can be briefly divided into two parts. The first term is related to the space arrangement of particles, independent of the pressure field. It can be regarded as a coefficient of renormalization that is denoted by the symbol  $C_i^{-1}$

$$C_i = \frac{1}{n_0} \sum_{i \neq j} w(|\mathbf{r}_j - \mathbf{r}_i|) \frac{(\mathbf{r}_j - \mathbf{r}_i)}{|\mathbf{r}_j - \mathbf{r}_i|} \otimes \frac{(\mathbf{r}_j - \mathbf{r}_i)^T}{|\mathbf{r}_j - \mathbf{r}_i|} \quad (27)$$

$C_i$  is an  $N \times N$  matrix, and  $N$  is equal to the space dimension. Provided that the inverse of matrix  $C_i$  exists,  $\det(C_i)$  cannot be zero. However,  $\det(C_i)$  is likely to be zero in some special cases. As shown in Figure 3, for example, there is only single particle around the target particle in the actuating range of kernel function. Under this circumstance, Eq. (26) is out of operation. The reason is that when the two space vectors are introduced to the Taylor expansion of the gradient equation, the nonzero assumption of each vector is guaranteed but the product of the two vectors is not. This problem also exists in predecessor's gradient operators that are derived from the Taylor series expansion [20, 25, 33]. To resolve this problem, an integrated pressure gradient model is constituted as follows:

$$\nabla p|_i = \begin{cases} \left[ \frac{1}{n_0} \sum_{i \neq j} w(|\mathbf{r}_j - \mathbf{r}_i|) \frac{(\mathbf{r}_j - \mathbf{r}_i)}{|\mathbf{r}_j - \mathbf{r}_i|} \otimes \frac{(\mathbf{r}_j - \mathbf{r}_i)^T}{|\mathbf{r}_j - \mathbf{r}_i|} \right]^{-1} \left[ \frac{1}{n_0} \sum_{i \neq j} w(|\mathbf{r}_j - \mathbf{r}_i|) \frac{p_j - \hat{p}_i}{|\mathbf{r}_j - \mathbf{r}_i|} (\mathbf{r}_j - \mathbf{r}_i) \right] & \det(C_i) \geq 0.05 \\ \frac{D_s}{n_0} \sum_{i \neq j} w(|\mathbf{r}_j - \mathbf{r}_i|) \frac{p_j - \hat{p}_i}{|\mathbf{r}_j - \mathbf{r}_i|} (\mathbf{r}_j - \mathbf{r}_i) & \det(C_i) < 0.05 \end{cases} \quad (28)$$

When  $\det(C_i)$  is less than a critical value, the original pressure gradient model is used instead of Eq.(26). Here, 0.05 is recommended as the critical value, which is obtained by trial and error. Equation (28) is effective to avoid numerical errors caused by a singular matrix, and here, it is named as the combined pressure gradient model.

Through the following numerical tests, the corrected gradient operator is demonstrated to improve the energy conservation of the original algorithm. The introduction of the minimum pressure in the corrected gradient model contributes to the numerical stability of the MPS method.

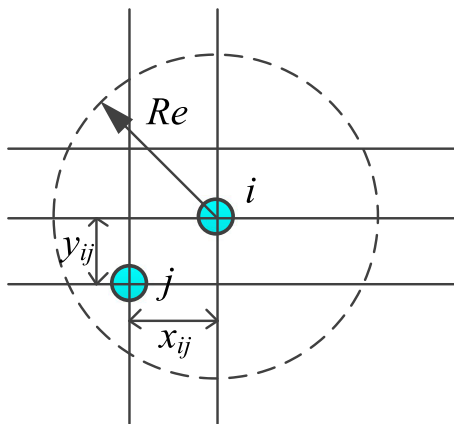


Figure 3. A special situation of particles layout. [Colour figure can be viewed at [wileyonlinelibrary.com](http://wileyonlinelibrary.com)]

### 3. NUMERICAL RESULTS AND DISCUSSIONS

#### 3.1. Simulation of hydrostatic pressure problem

The improved MPS method is firstly tested in the simulation of a hydrostatic problem as shown in Figure 4 where a static water column of 0.4 m in width and 0.4 m in height is initially set up in a water tank. Totally, 1600 particles with a diameter of 0.01 m were used in the calculation. The calculated pressure at 0.02 m above the bottom in the middle of the tank is recorded to examine its temporal variations. It is verified that the proposed new surface detection method and the corrected pressure gradient model have obvious contribution to the numerical stability of the MPS method.

The proposed surface identification criterion is compared with the original method by using particle number density and that with the neighboring particle number. Table I lists the calculation condition.

Figure 5 gives comparisons of the temporal variations of the calculated fluid pressure at point A by using different surface identification methods, and Figure 6 is the corresponding relative error rate of pressure that is defined by following Eq. (29).

$$RER = \frac{P_i - P_{analytic}}{P_{analytic}} \quad (29)$$

It can be seen from these figures that comparing with the results obtained by using value of particle pressure (VPP) and number of neighbor particles (NNP) criteria for surface particles, there exists remarkable fluctuation in the time history of calculated fluid pressure if only particle number density (PND) criterion is used. And the maximum value of relative error rate exceeds 100% which means the calculated pressure can be two times of the static pressure. In contrast, the bias error of

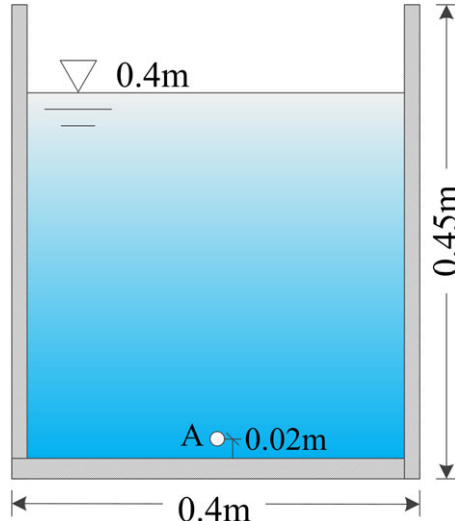


Figure 4. Schematic diagram of a hydrostatic pressure problem. [Colour figure can be viewed at [wileyonlinelibrary.com](http://wileyonlinelibrary.com)]

Table I. Surface detection methods applied in this study.

Surface detection method	Abbreviation	Description
Identification with particle number density	PND criterion	Only use Eq.(11)
Identification with the number of neighbor particles	NNP criterion	Use Eqs (11) and (12)
Identification with the value of particle pressure	VPP criterion	Use Eqs (11) and (13)

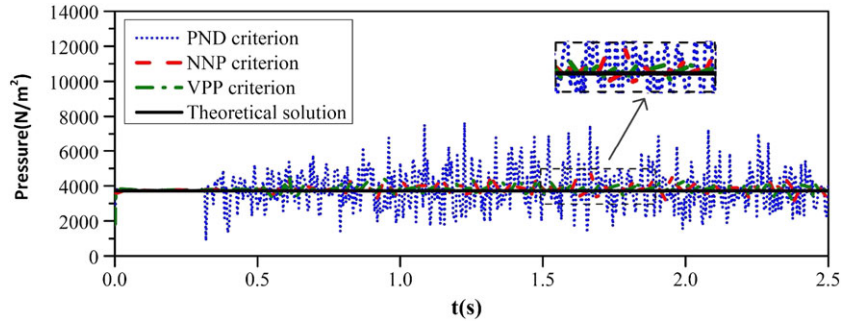


Figure 5. Comparison of the calculated fluid pressure at point A with different surface detection methods. NNP, number of neighbor particles; PND, particle number density; VPP, value of particle pressure. [Colour figure can be viewed at [wileyonlinelibrary.com](http://wileyonlinelibrary.com)]

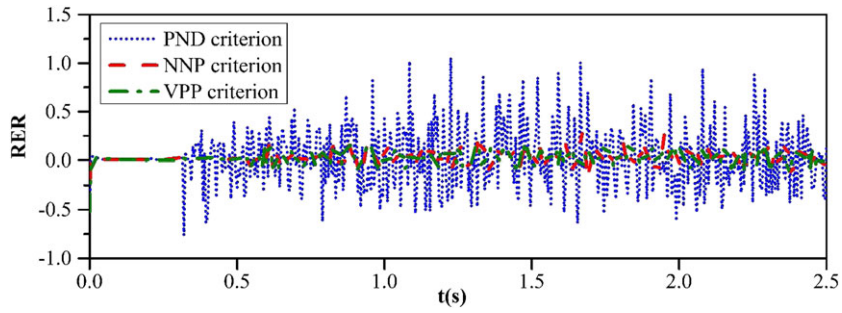


Figure 6. Comparison of the relative error rate of pressure at point A with different surface detection methods. NNP, number of neighbor particles; PND, particle number density; VPP, value of particle pressure. [Colour figure can be viewed at [wileyonlinelibrary.com](http://wileyonlinelibrary.com)]

the calculated pressure is obviously controlled with both VPP and NNP criteria. For instance, the maximum error by VPP criterion is about 20% which is less than that by NNP criterion (more than 25%). It can be concluded that the misrecognition of surface particles is one of the major factors causing the nonphysical pressure oscillation.

Except for the hydrostatic water problem, the new free surface particle detection method with pressure is verified to be effective for the simulation of violent flows with significant free surface variations. As another example, the comparison of the simulated water motion of dam breaking with the criteria of PND and VPP is visualized in Figure 7, in which the red points represent surface particles and the green points denote inner fluid particles. As seen from Figure 7, the simulated result by VPP criterion Figure 7(b) is much better than that by PND criterion, indicating that the proposed VPP criterion is qualified to alleviate the misrecognition of free surface particles. However, the new surface detection criterion has little improvement on the surface particles of the splash-up water from the main body in which the pressure field is not consecutive any more. Because in the typical MPS algorism the inner particles are involved in solving PPE while the surface particles are identified by the Dirichlet boundary condition, the misrecognition of surface particles may seriously damage the accuracy of the calculated pressure field.

On the other hand, the effectiveness of the new proposed gradient model is illustrated by the following results. Figure 8 shows the calculated time history of pressure at point A by using the different gradient models that are illustrated in Table II. The new surface particle identification criterion (VPP criterion) is applied in the calculation. It shows that the calculated result by new combined gradient model with the consideration of minimum pressure agrees well with the analytical solution and is much better than that by the other gradient models.

Figure 9 gives the comparison of temporal variation in the particle number density at point A between the new combined gradient model and the general Taylor series gradient model. It can

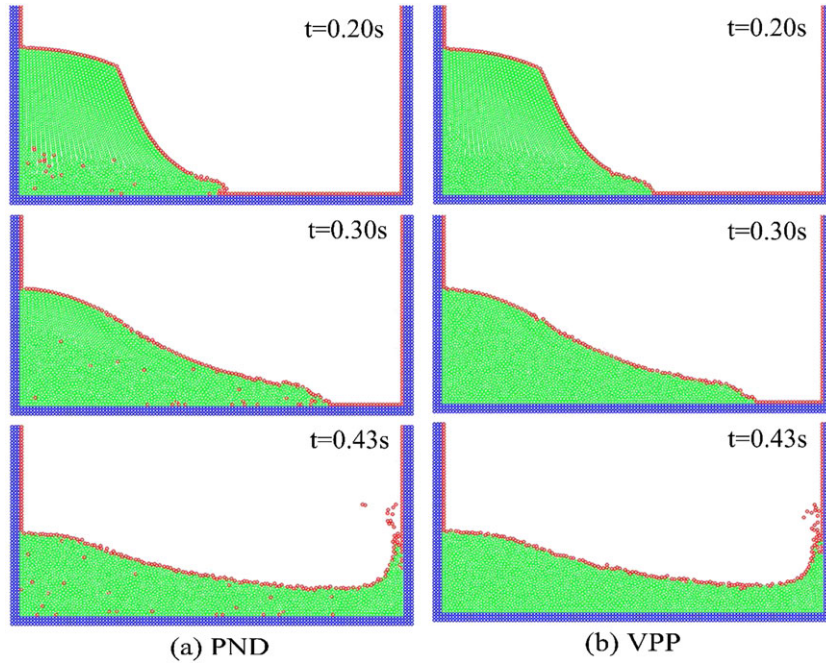


Figure 7. Snapshots of free surface particles in the calculation of dam breaking by traditional and new surface detection methods, respectively. PND, particle number density; VPP, value of particle pressure.  
[Colour figure can be viewed at [wileyonlinelibrary.com](http://wileyonlinelibrary.com)]

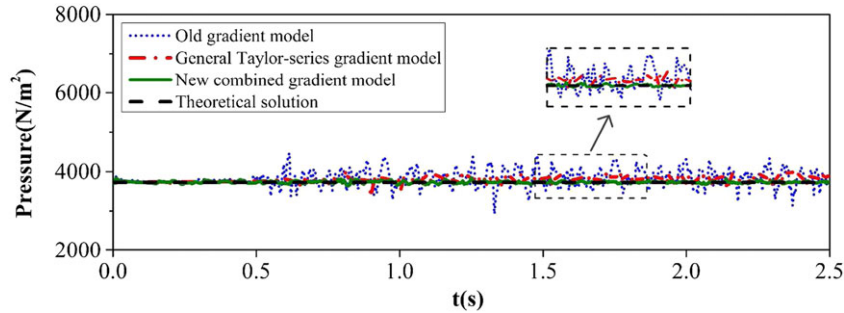


Figure 8. Time history of pressure at point A calculated with different gradient models. [Colour figure can be viewed at [wileyonlinelibrary.com](http://wileyonlinelibrary.com)]

Table II. The statement of pressure gradient models used in the calculations.

Pressure gradient model	Abbreviation	Description
The pressure gradient model proposed by Kozhizuka <i>et al.</i>	Old gradient model	Eqs (15) and (16)
The Taylor series consistent pressure gradient model without the minimum pressure	General Taylor series gradient model	Eq. (24)
The combined pressure gradient model proposed in this paper	New combined gradient model	Eqs (28) and (16)

be seen that by adding the minimum pressure in the new gradient model, the bias error of calculated particle number density tends to be nearly zero and stable. Without minimum pressure, the density variation is of the opposite trend, which means that the local clustering gets serious. The comparison of the new coupling gradient model and the general Taylor series gradient model indicates that

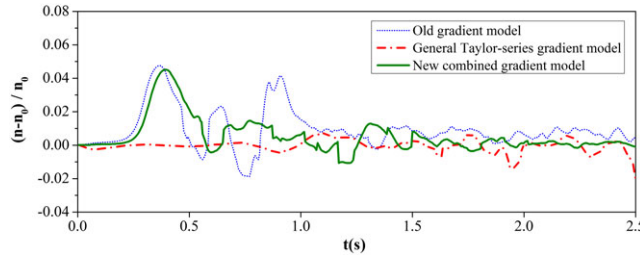


Figure 9. Comparison of the calculated time variation of particle number density at point A. [Colour figure can be viewed at [wileyonlinelibrary.com](http://wileyonlinelibrary.com)]

the consideration of surrounding minimum pressure contributes to the improvement of the MPS algorithm stability.

### 3.2. Simulation of regular sinusoidal waves

It has been pointed out that there exists severe numerical wave attenuation in the calculation of wave propagations by the original MPS model, which is especially notable in the simulation of regular sinusoidal waves. The corrected MPS model is verified to be appropriate to amend this problem by the following example. In Table III, the calculation conditions for four different study cases are listed in terms of the different combination of gradient models and surface particle detection methods. Figure 10 is the schematic diagram of the wave flume. The initial wave height is 0.8 m, and the wave period is 2.54 s. In the calculation, the diameter of a particle is given as  $l_0 = 0.1$ , and totally, 14,240 particles are used. The time step is determined by Courant–Friedrichs–Lewy stability condition, and the maximum value is chosen as 0.008 s.

A flap-type of wave paddle is used to generate waves, and its movement is governed by Eq. (30) that is derived from the linear wave maker theory

$$U = \frac{\omega}{W^\#} \eta \quad (30)$$

Table III. Study cases and calculation conditions.

Cases	Gradient model	Surface detection method
Case 1	Eq.(15)	Only Eq.(11)
Case 2	Eq.(15)	Eqs (11) and (13)
Case 3	Eq.(24)	Eqs (11) and (13)
Case 4	Eq.(28)	Eqs (11) and (13)

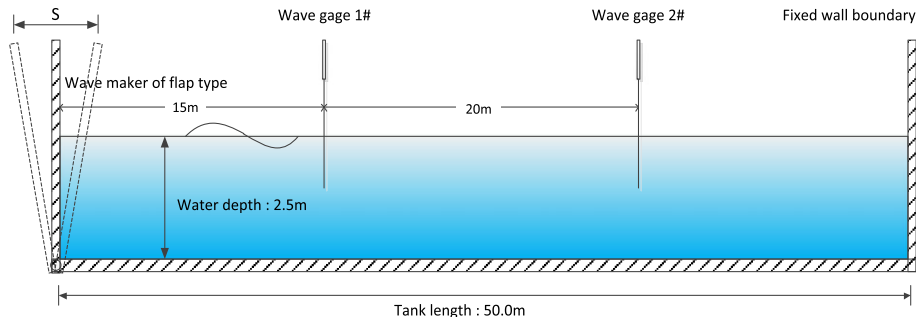


Figure 10. Schematic diagram of numerical wave flume. [Colour figure can be viewed at [wileyonlinelibrary.com](http://wileyonlinelibrary.com)]

Here,  $\omega$  is the wave angular frequency,  $\eta$  is a surface elevation  $\eta = A\cos(\omega t)$ ,  $A$  is wave amplitude, and  $W^\#$  is a hydraulic transfer function, which equals to the ratio of wave height to stroke.  $W^\#$  is defined as

$$W^\# = 4 \left( \frac{\sinh kh}{kh} \right) \frac{kh \sinh kh - \cosh kh + 1}{\sinh 2kh + 2kh} \quad (31)$$

where  $k$  is the wave number and  $h$  is the water depth.

Figure 11 is the snapshots showing the simulated wave propagation along a wave flume at different times for the four different cases. Figure 12 gives the comparison of corresponding wave height

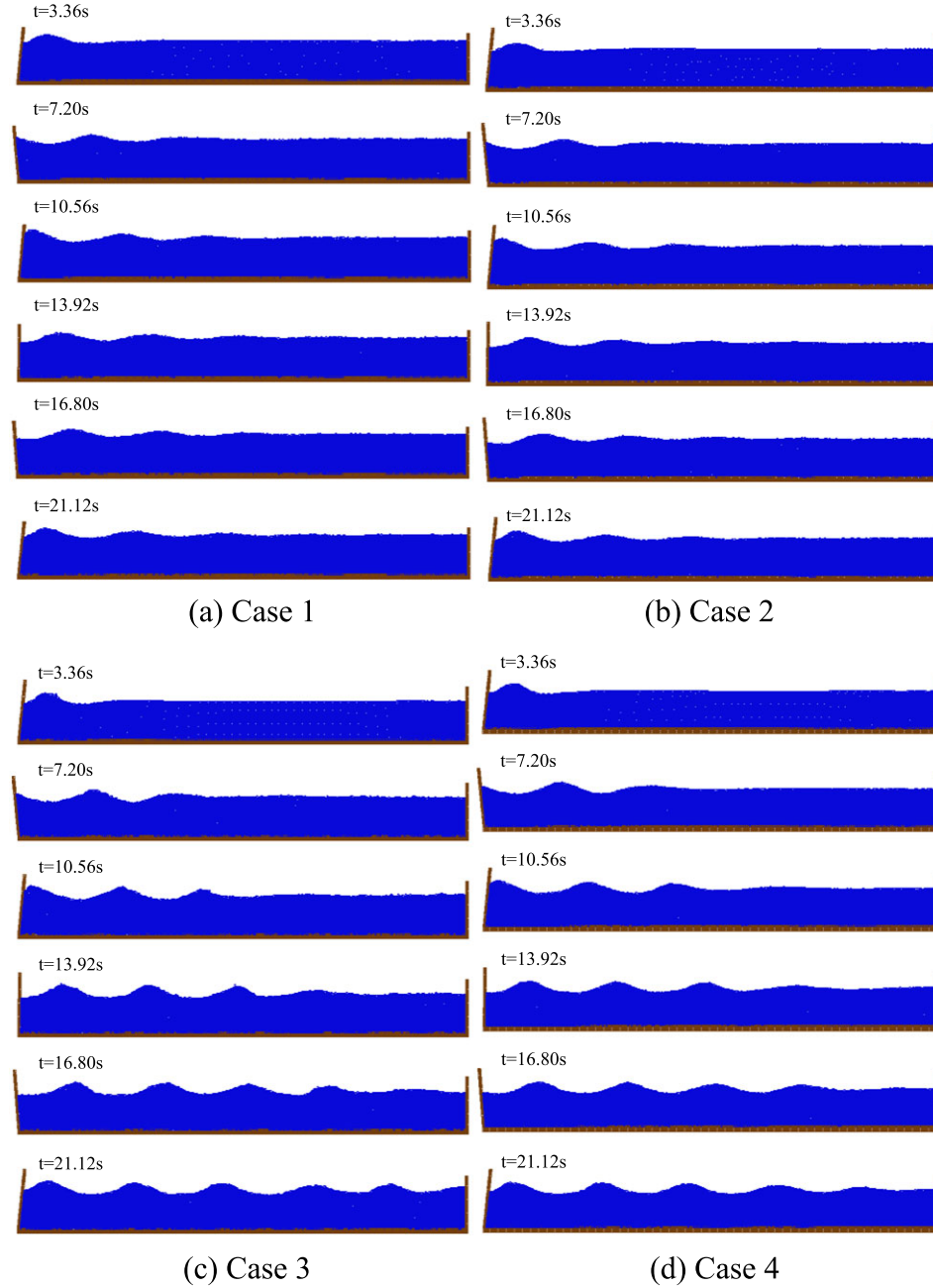


Figure 11. Comparison of the calculated wave fields of different cases. (a) Case 1, (b) Case 2, (c) Case 3, and (d) Case 4. [Colour figure can be viewed at [wileyonlinelibrary.com](http://wileyonlinelibrary.com)]

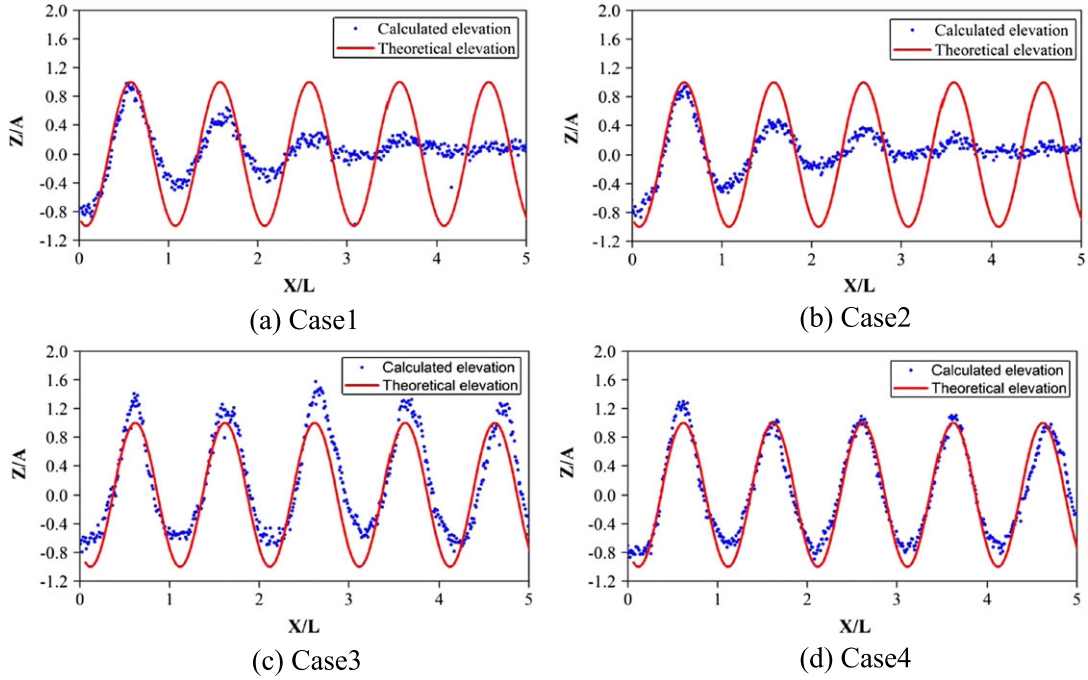


Figure 12. Comparison of wave height distribution along wave flume (at  $t = 26.88$  s). The symbols A and L are the abbreviations of wave amplitude and wavelength, respectively. (a) Case1, (b) Case2, (c) Case3, and (d) Case4. [Colour figure can be viewed at [wileyonlinelibrary.com](http://wileyonlinelibrary.com)]

distribution along the wave flume between the calculation and analytical solution after about 10 wave cycles. From Figures 11(a)(b) and 12(a)(b), it can be seen that the generated waves from wave paddle can only transmit to two or three wavelengths and very large numerical wave attenuation exists in Cases 1 (the original gradient model and surface detection criterion) and 2 (the original gradient model with the new surface detection criterion). This indicates that the numerical wave attenuation is unavoidable with the original gradient model, and it cannot be effectively eliminated only by the new surface particle detection criterion. However, as shown in Figures 11(d) and 12(d) of Case 4 (the improved gradient model with the minimum pressure and new surface detection criterion), the numerical wave dissipation has been drastically decreased by using the new gradient model. It is necessary to point out that although Figure 11(c) of Case 3 (the improved gradient model without the minimum pressure and new surface detection criterion) also shows a reduction in the numerical wave damping, comparing Figure 12(c) with Figure 12(d), the calculated wave height distribution along wave flume in Case 3 is obviously bad and does not agree with the analytical solution.

Figure 13 is the comparison of the calculated time history of water surface elevation at  $x = 15.0$  m and  $x = 35.0$  m far from wave paddle obtained in Cases 3 and 4. It also verified that with the

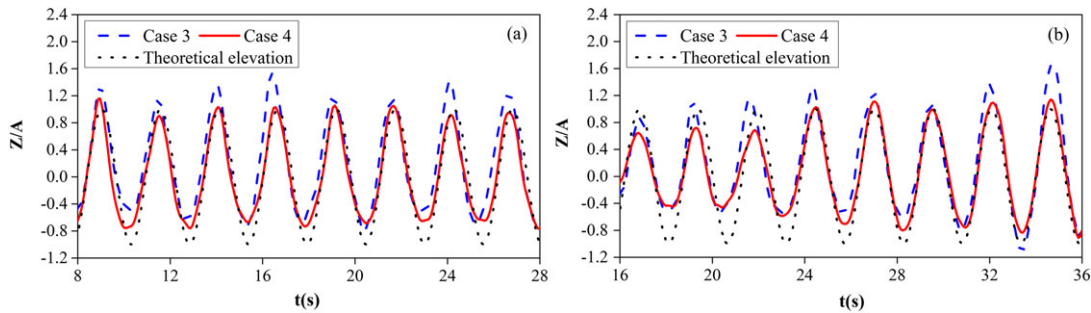


Figure 13. Comparison of the calculated water surface elevation with analytical solution (a) at  $x = 15.0$  m and (b) at  $x = 35.0$  m. [Colour figure can be viewed at [wileyonlinelibrary.com](http://wileyonlinelibrary.com)]

consideration of the surrounding minimum pressure in the gradient model, the calculated wave profile is more stable and agrees well with the theoretical result.

Figure 14 gives the calculated pressure and velocity fields at  $t = 26.88$  s in the four different cases where the enlarged part is the local velocity fields. The distributions of local velocity and pressure obtained in Case 4 by using the improved MPS model are much better than those in the other Cases. Through comparisons of the calculated velocity fields, it can be understood that during the calculation in the study Cases 1 and 2, large part of the kinetic energy for the large-scale wave propagation are consumed by the small-scale random fluctuation resulting in the numerical wave energy

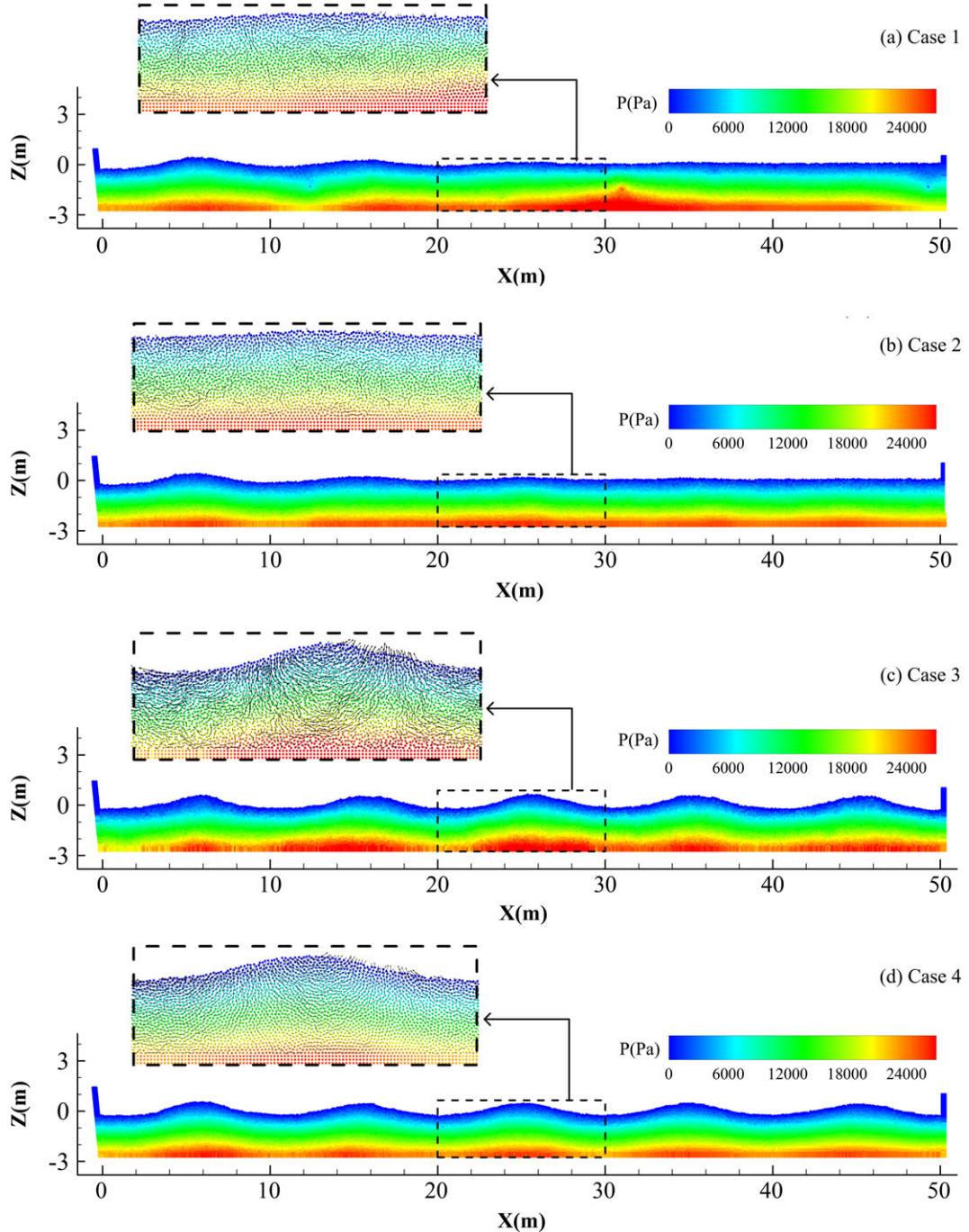


Figure 14. The calculated pressure and velocity fields with different gradient model at  $t = 26.88$  s. (a) Case 1, (b) Case 2, (c) Case 3, and (d) Case 4. [Colour figure can be viewed at [wileyonlinelibrary.com](http://wileyonlinelibrary.com)]

dissipation along the wave flume, and the dominant reason for this serious numerical wave damping is due to the poor accuracy of the gradient operators.

### 3.3. Simulation of a standing wave

A two-dimensional standing wave in a rectangular tank is simulated to investigate the energy conservation properties of the improved MPS method [28, 35]. The water depth  $h$  is 0.8 m, and the bottom width is 2 m. The initial configuration of the free surface is given as (Figure 15):

$$\eta_0(x, t) = A \cos[k(x + \lambda/2)] \quad (32)$$

where  $\eta_0$  is the initial surface elevation,  $A = 0.1$  m is the wave amplitude,  $\lambda = 2$  m is the wavelength, and  $k = 2\pi/\lambda$  is the wave number. The wavelength is set to be equal to the width of the tank. The particle size  $l_0 = 0.01$  m and 17,205 particles are used in the calculation. The maximum time step is 0.001 s. In the beginning, velocities of all particles are set as zero.

Figure 16 gives the time histories of the water surface elevation at the center of the rectangular tank ( $x = 1.0$  m), which are calculated by the original and present MPS methods, respectively, and the numerical results are compared with the second-order analytical solution of Wu and Taylor [40]. The comparison manifests that the phenomenon of wave damping in the original MPS model is considerably serious. By contrast, the agreement between the present result and the analytical solution is much better. Figure 17 shows the pressure distributions of the standing wave at  $t = 3.44$  s. The results demonstrate that the improved MPS model contributes to the enhancement of the energy

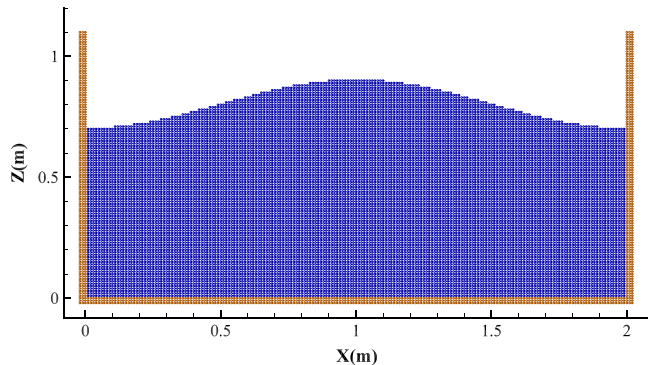


Figure 15. Initial condition of the standing wave. [Colour figure can be viewed at [wileyonlinelibrary.com](http://wileyonlinelibrary.com)]

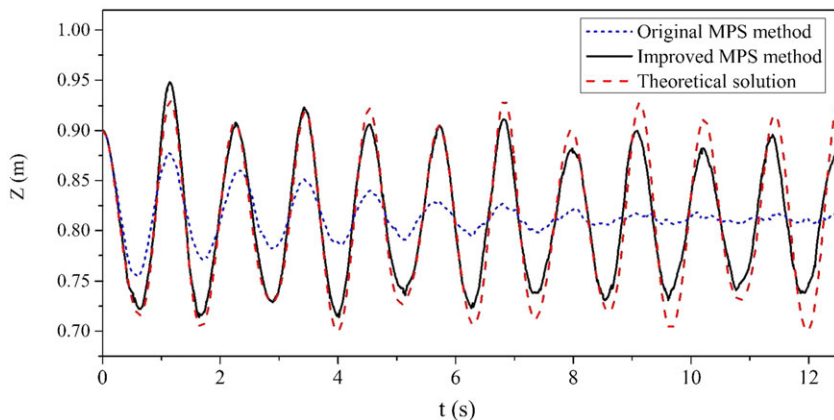


Figure 16. Time histories of the water surface elevation at the center of the tank simulated by the original and improved moving particle semi-implicit (MPS) methods, respectively. [Colour figure can be viewed at [wileyonlinelibrary.com](http://wileyonlinelibrary.com)]

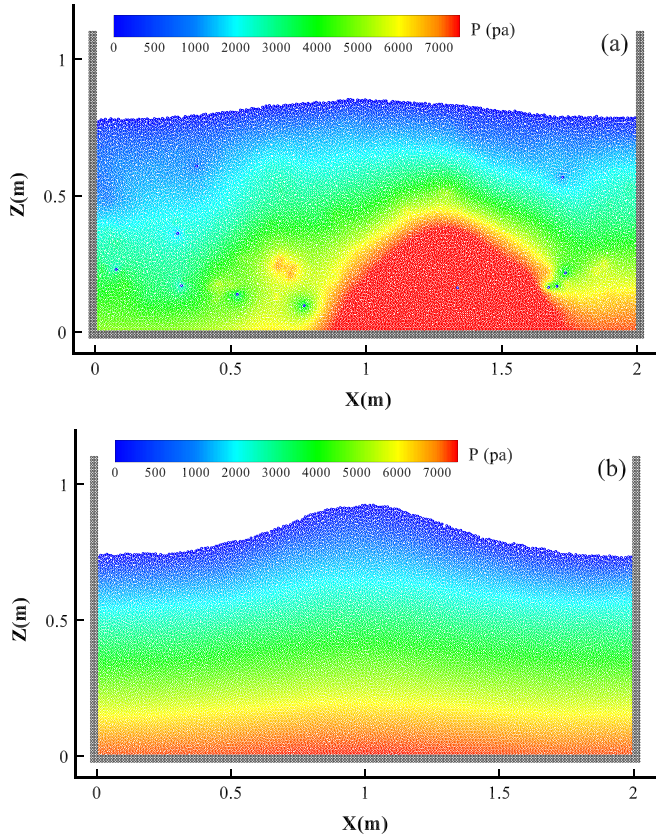


Figure 17. Snapshots of pressure fields simulated by the moving particle semi-implicit (MPS) models at  $t = 3.44$  s. (a) Original MPS method; (b) Improved MPS method. [Colour figure can be viewed at [wileyonlinelibrary.com](http://wileyonlinelibrary.com)]

conservation. However, the slight wave damping still exists in the present model, which can be amended in the future study.

### 3.4. Simulation of solitary wave plunging on a slope

As another important type of progressive waves, solitary waves are likewise of importance in the research of coastal engineering, particularly the exploration of solitary wave breaking. The plunging breaking of solitary wave involves strong nonlinear characteristics, which bring about many mathematical problems beyond the theoretical description. From the given examples, the improved MPS method has a significant superiority in the simulation of fragmentation and coalescence of fluid. Its application for the simulation of plunging breaking of a solitary wave on the slope is discussed in the following. A schematic drawing of the computation domain is depicted in Figure 18. In this case, the size of a particle is 0.005 m, and the time step is 0.001 s. The moving wall is used to generate solitary waves, and the starting point of the slope in Figure 18 is set at the position  $x = 1.5$  m. The slope is 1:15 and water depth  $h_0$  is 0.2 m. According to the breaking type of solitary wave defined by Grill *et al.* [4], the relative height  $H_0/h_0$  is set as 0.4 for achieving the plunging breaking. The profile of a solitary wave can be expressed as a function of distance  $x$  and time  $t$ :

$$\eta(x, t) = H_0 \operatorname{sech}^2[n(x - Ct)] \quad (32)$$

where  $C$  is the wave velocity,  $H_0$  is the incident wave height, and  $n$  is given by

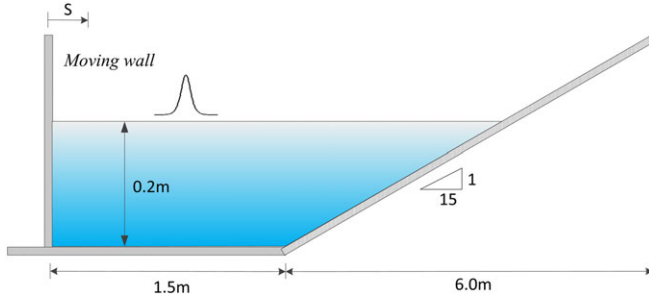


Figure 18. A schematic presentation of wave propagation on the slope. [Colour figure can be viewed at [wileyonlinelibrary.com](http://wileyonlinelibrary.com)]

$$n = \sqrt{\frac{3H_0}{4h_0^3}} \quad (33)$$

Before discussing the solitary wave propagation over the sloping bed, the improved MPS model is calibrated by an example of a solitary wave travelling on a flat bottom through comparisons of the old and present model results with the analytical solution as shown in Figure 19. It is found from Figure 19 that the general tendency of the numerical wave damping for the solitary wave propagating along a flat bottom is much smaller than that for the regular sinusoidal waves by both old and improved MPS models. But with the old MPS model as shown in Figure 19(a), the numerical wave attenuation is still quite bigger and the wave shapes deform severely. As a contrast, as seen in Figure 19(b), the numerical wave damping by the present MPS model is remarkably decreased with an enhancement in the accuracy of the algorithm. And the generated solitary wave with the new MPS model is in general agreement with the analytical solution, even though the slight wave

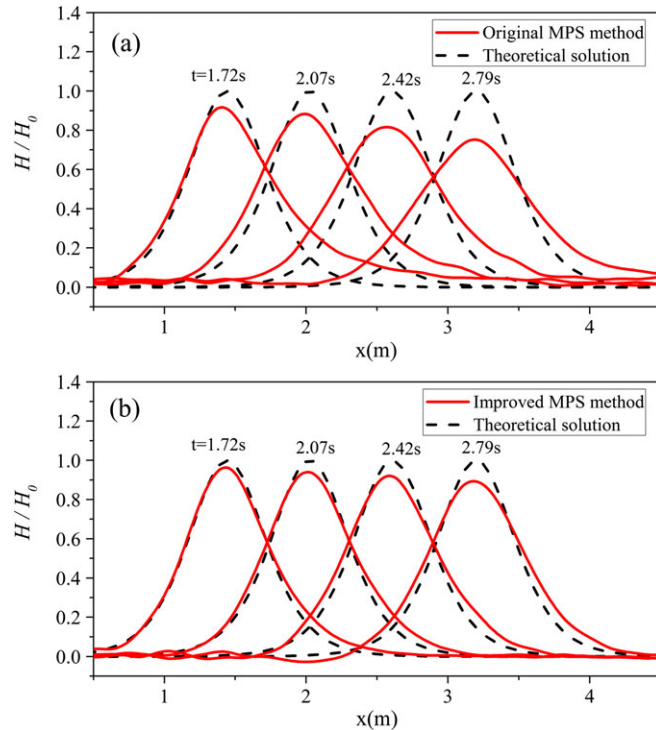


Figure 19. Profiles of the solitary wave travelling on a flat bottom at different moments. MPS, moving particle semi-implicit. [Colour figure can be viewed at [wileyonlinelibrary.com](http://wileyonlinelibrary.com)]

attenuation still exists, which may be in part caused by the trailing wave train observed in Figure 19 (b). As reported by other researchers [41, 42], the trailing wave train occurring behind the main water body takes away some energy and causes the decrease of the solitary wave height.

The calculated process of a solitary wave plunging breaking on the sloping bed is presented meticulously in Figure 20. The left snapshots are the results simulated with the original MPS method, and the right snapshots are obtained by the improved MPS method. The two sets of results are simultaneously contrasted with the Li's laboratory experiment results [43], the photos in the middle. It is apparent that the results calculated by the improved MPS method are more qualitatively well identical with the experiment results. The development of plunging jet is precisely represented, and the profiles of cavities are distinct and smoothed in the right pictures. Besides, the highly nonlinear splash-up process of water is reproduced well. Although the original MPS is capable of simulating the wave breaking, its results are inferior to that of the corrected MPS, as given on the left in which the shapes of the cavities are obviously different from that in the experiment at the early stages of plunging breaking, and the cavity vanishes quickly as the post-breaking proceeds. But frankly, in spite of the good simulation of the whole process by the present MPS model, there exist some minor disagreements between the simulated snapshots and the laboratory photographs.

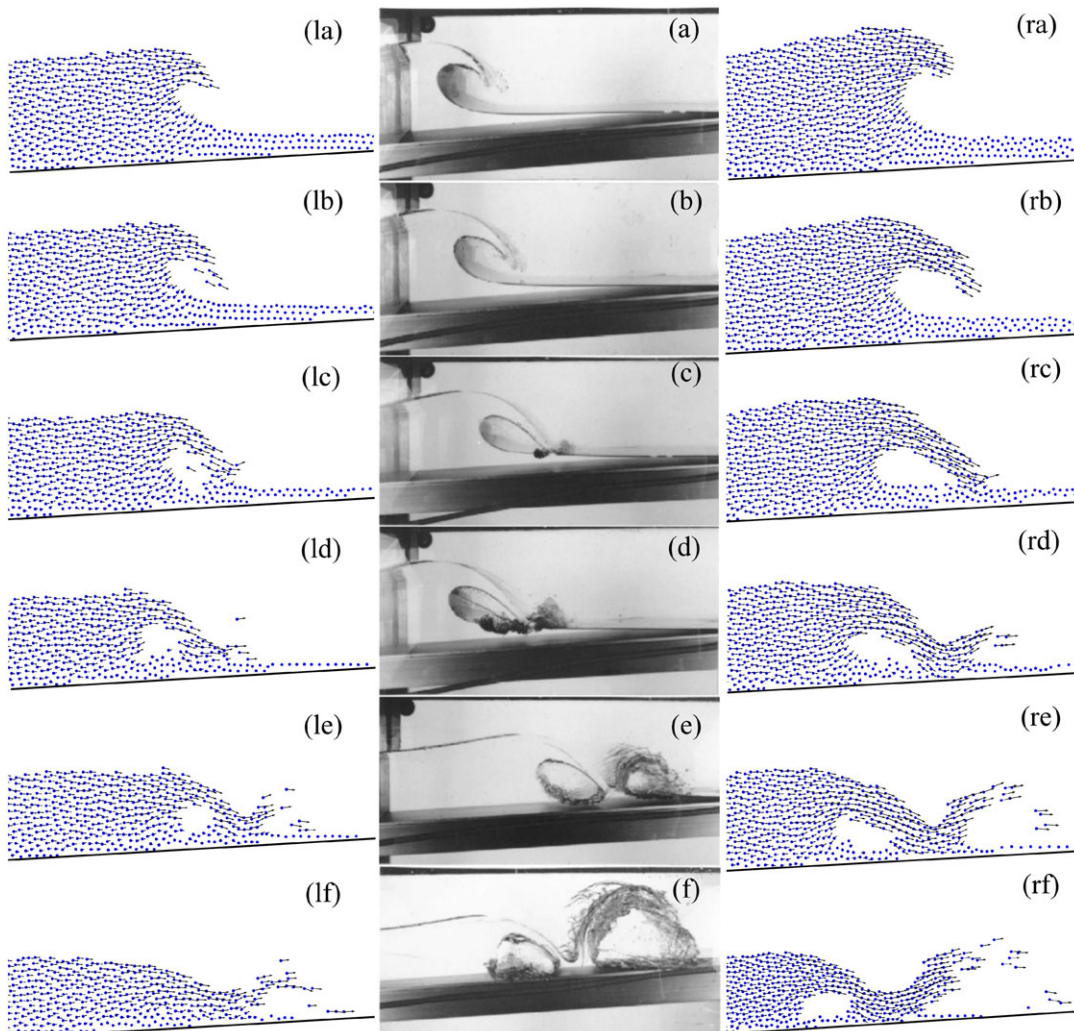


Figure 20. The descriptions of plunging breaking and splash-up of solitary wave interacting with a slope. The left is the result of old moving particle semi-implicit method, the right is the improved moving particle semi-implicit, and the middle is Li's experimental result. [Colour figure can be viewed at [wileyonlinelibrary.com](http://wileyonlinelibrary.com)]

For instance, the height of reflected jet is less than that in the experiment, and the particles unevenly hang down, which all need to be revised in the future.

#### 4. CONCLUSIONS

In this study, a simple surface particle detection criterion in terms of water pressure is proposed, and a new gradient model with consideration of the surrounding minimum pressure is derived from Taylor series expansion analysis. Through the applications to the hydrostatic pressure problem and the propagation of progressive waves, it is verified that the proposed surface particle identification criterion is effective to reduce the particle misrecognition and then beneficial to suppress the nonphysical pressure oscillation. Another conclusion is that the new combined gradient model is useful to keep the energy conservation and to reduce the numerical wave dissipation. It is clarified that the particle clustering and nonphysical pressure fluctuation can be further reduced through introducing the surrounding minimum pressure term in the proposed gradient model. Moreover, the simulation of a standing wave further demonstrates the enhancement of energy conservation in the corrected MPS model. In a word, the modifications on the original MPS method are helpful to enhance the stability of the algorithm and its accuracy for the simulation of progressive water waves. The improved MPS method prepares well for the future numerical research of the interaction between waves and structures.

#### ACKNOWLEDGEMENT

This study is supported by the Fundamental Research Funds for the Central Universities of China (2013B31514 and 2014B31014) and the National Natural Science Foundation of China (51479056).

#### REFERENCES

1. Cointe R. Numerical simulation of a wave channel. *Engineering Analysis with Boundary Elements* 1990; **7**(4):167–177.
2. Dodd N. Numerical model of wave run-up, overtopping, and regeneration. *Journal of Waterway Port Coastal and Ocean Engineering-ASCE* 1998; **124**(2):73–81.
3. Li Y, Raichlen F. Non-breaking and breaking solitary wave run-up. *Journal of Fluid Mechanics* 2002; **456**:295–318.
4. Grilli ST, Svendsen IA, Subramanya R. Breaking criterion and characteristics for solitary waves on slopes. *Journal of Waterway Port Coastal and Ocean Engineering-ASCE* 1997; **123**(3):102–112.
5. Loubère R, Maire P, Shashkov M, Breil J, Galera S. ReALE: A reconnection-based arbitrary-Lagrangian–Eulerian method. *Journal of Computational Physics* 2010; **229**(12):4724–4761.
6. Lee K, Leap DI. Simulation of a free-surface and seepage face using boundary-fitted coordinate system method. *Journal of Hydrology* 1997; **196**(1–4):297–309.
7. Nakayama T, Mori M. An Eulerian finite element method for time-dependent free surface problems in hydrodynamics. *International Journal for Numerical Methods in Fluids* 1996; **22**(3):175–194.
8. Christakos N, Allsop N, Beale RG, Cooper AJ, Dennis JM. A volume of fluid numerical model for wave impacts at coastal structures. *Proceedings of the Institution of Civil Engineers-Water and Maritime Engineering* 2002; **154**(3):159–168.
9. Liu D, Lin P. Three-dimensional liquid sloshing in a tank with baffles. *Ocean Engineering* 2009; **36**(2):202–212.
10. Sussman M, Smereka P, Osher S. A level set approach for computing solutions to incompressible two-phase flow. *Journal of Computational Physics* 1994; **114**(1):146–159.
11. Sun DL, Tao WQ. A coupled volume-of-fluid and level set (VOSET) method for computing incompressible two-phase flows. *International Journal of Heat and Mass Transfer* 2010; **53**(4):645–655.
12. Jemison M, Loch E, Sussman M, Shashkov M, Arienti M, Ohta M, et al. A coupled level set-moment of fluid method for incompressible two-phase flows. *Journal of Scientific Computing* 2013; **54**(2–3):454–491.
13. Hirt CW, Nichols BD. Volume of fluid (VOF) method for the dynamics of free boundaries. *Journal of Computational Physics* 1981; **39**(1):201–225.
14. Moraghan JJ. Smoothed particle hydrodynamics: theory and applications to non-spherical stars. *Manual Notebook of Royal Astronomical Society* 1977.
15. Koshizuka S, Oka Y. Moving-particles semi-implicit method for fragmentation of incompressible fluid. *Nuclear Science and Engineering* 1996; **123**:421–434.
16. Leroy A, Violeau D, Ferrand M, Kassiotis C. Unified semi-analytical wall boundary conditions applied to 2-D incompressible SPH. *Journal of Computational Physics* 2014; **261**:106–129.

17. Shibata K, Koshizuka S, Sakai M, Tanizawa K. Lagrangian simulations of ship-wave interactions in rough seas. *Ocean Engineering* 2012; **42**:13–25.
18. Shibata K, Koshizuka S. Numerical analysis of shipping water impact on a deck using a particle method. *Ocean Engineering* 2007; **34**(3–4):585–593.
19. Koshizuka S, Nobe A, Oka Y. Numerical analysis of breaking waves using the moving particle semi-implicit method. *International Journal for Numerical Methods in Fluids* 1998; **26**(7):751–769.
20. Khayyer A, Gotoh H, Shao SD. Corrected incompressible SPH method for accurate water-surface tracking in breaking waves. *Coastal Engineering* 2008; **55**(3):236–250.
21. Khayyer A, Gotoh H. Development of CMPS method for accurate water-surface tracking in breaking waves. *Coastal Engineering Journal* 2008; **50**(2):179–207.
22. Shibata K, Koshizuka S, Sakai M, Tanizawa K. Transparent boundary condition for simulating nonlinear water waves by a particle method. *Ocean Engineering* 2011; **38**(16):1839–1848.
23. Antuono M, Colagrossi A, Marrone S, Lugni C. Propagation of gravity waves through an SPH scheme with numerical diffusive terms. *Computer Physics Communications* 2011; **182**(4):866–877.
24. Jian W, Sim SY, Huang Z, Lo EY. Modelling of solitary wave run-up on an onshore coastal cliff by smoothed particle hydrodynamics method. *Procedia Engineering* 2015; **116**:88–96.
25. Khayyer A, Gotoh H. Enhancement of performance and stability of MPS mesh-free particle method for multiphase flows characterized by high density ratios. *Journal of Computational Physics* 2013; **242**:211–233.
26. Khayyer A, Gotoh H. Enhancement of stability and accuracy of the moving particle semi-implicit method. *Journal of Computational Physics* 2011; **230**(8):3093–3118.
27. Kondo M, Koshizuka S. Improvement of stability in moving particle semi-implicit method. *International Journal for Numerical Methods in Fluids* 2011; **65**(6):638–654.
28. Suzuki Y, Koshizuka S, Oka Y. Hamiltonian moving-particle semi-implicit (HMPS) method for incompressible fluid flows. *Computer Methods in Applied Mechanics and Engineering* 2007; **196**(29–30):2876–2894.
29. Tanaka M, Masunaga T. Stabilization and smoothing of pressure in MPS method by quasi-compressibility. *Journal of Computational Physics* 2010; **229**(11):4279–4290.
30. Lee B, Park J, Kim M, Hwang S. Step-by-step improvement of MPS method in simulating violent free-surface motions and impact-loads. *Computer Methods in Applied Mechanics and Engineering* 2011; **200**(9–12):1113–1125.
31. Chen X, Xi G, Sun Z. Improving stability of MPS method by a computational scheme based on conceptual particles. *Computer Methods in Applied Mechanics and Engineering* 2014; **278**:254–271.
32. Khayyer A, Gotoh H. A higher order Laplacian model for enhancement and stabilization of pressure calculation by the MPS method. *Applied Ocean Research* 2010; **32**(1):124–131.
33. Iribe T, Nakaza E. A precise calculation method of the gradient operator in numerical computation with the MPS (in Japanese). *Journal of JSCE, Ser B2 (Coastal Engineering)* 2010; **66**(1):46–50.
34. Gotoh H, Khayyer A, Ikari H, Shimizu Y. Wave propagation simulation by accurate mps method with high energy conservation property (in Japanese). *Journal of JSCE, Ser B2 (Coastal Engineering)* 2015; **71**(2):25–30.
35. Gotoh H, Khayyer A. Current achievements and future perspectives for projection-based particle methods with applications in ocean engineering. *Journal of Ocean Engineering and Marine Energy* 2016; **2**(3):251–278.
36. Khayyer A, Gotoh H, Shao S. Enhanced predictions of wave impact pressure by improved incompressible SPH methods. *Applied Ocean Research* 2009; **31**(2):111–131.
37. Zhang Y, Wan D, Hino T. Comparative study of MPS method and level-set method for sloshing flows. *Journal of Hydrodynamics, Ser. B* 2014; **26**(4):577–585.
38. Toyota E, Kubo HAS. A particle method with variable spatial resolution for incompressible flows. *19th Japan Society of Fluid Mechanics* 2005.
39. Tsuruta N, Khayyer A, Gotoh H. A short note on dynamic stabilization of moving particle semi-implicit method. *Computers & Fluids* 2013; **82**:158–164.
40. Wu GX, Taylor RE. Finite element analysis of two-dimensional non-linear transient water waves. *Applied Ocean Research* 1994; **16**(6):363–372.
41. Sun JL, Wang CZ, Wu GX, Khoo BC. Fully nonlinear simulations of interactions between solitary waves and structures based on the finite element method. *Ocean Engineering* 2015; **108**:202–215.
42. Huang CJ, Dong CM. On the interaction of a solitary wave and a submerged dike. *Coastal Engineering* 2001; **43**(3–4):265–286.
43. Li Y. Tsunamis: non-breaking and breaking solitary wave run-up, California Institute of Technology; 2000. Report No.: No. KH-R-60.